THE ROLE OF INFRARED THERMOGRAPHY IN THE STUDY OF CROSSFLOW INSTABILITY AT M=2.4

Simone Zuccher, William S. Saric, Helen L. Reed and Lloyd B. McNeil
Arizona State University, Tempe AZ 85287, USA

Keywords: *boundary-layer transition, instability, infrared thermography, control*

ABSTRACT

Distributed roughness located close to the leading edge of a swept wing can be used in order to accomplish drag reduction via passive laminar flow control (LFC). Past research at the Unsteady Wind Tunnel (UWT) of Arizona State University (ASU), has shown that laminar-to-turbulent boundary-layer transition in swept-wing flows and in low-disturbance environments can be controlled without the use of complicated systems. This idea is extended, in the present work, from low-speed to supersonic flows over highly swept wings at Mach number 2.4.

During this study infrared thermography (IRT) has been extensively exploited with very successful results. The main goal of this paper is to show that IRT is one of the most appropriate measurement/visualization techniques in order to detect transition. Furthermore, the possible problems and limitations encountered when dealing with IRT in high-speed flows are discussed.

1 INTRODUCTION

1.1 Crossflow Instability

Enabling laminar flow over most of the wing of a modern airplane would result in a remarkable engineering benefit. For this reason, transition to turbulence in crossflow-dominated, swept-wing boundary layers has received a considerable attention over the past decades. A recent review of swept wing stability by Saric et al. (2003) reports the results concerning the last years and complements the review by Reed and Saric (1989) about the work done during the 80s. Other recent efforts on crossflow instability are found in Arnal (1997), Bippes (1997, 1999), Crouch (1997), Haynes and Reed (2000), Herbert (1997a, 1997b), Kachanov (1996), Reibert and Saric (1997), Reshotko (1997), and Saric et al. (1998a,b).

The main difficulty encountered when considering crossflow instability is its strongly nonlinear nature and therefore the uselessness of linear methods in order to predict or control this specific instability. As far as incompressibility is concerned, it can be said that the primary crossflow instability is very well understood, including details of the nonlinear saturation of the dominant stationary mode and the growth of harmonics. As a consequence, Saric et al. (1998b) developed a technique of transition suppression, that utilizes the nature of the nonlinearities and uses distributed roughness in the vicinity of the leading edge in order to control transition.

It is well known that transition on a swept wing can be due to the combination of four basic instability mechanisms. Görtler instabilities (Saric 1994) can develop on concave curvature surfaces and therefore can be controlled by the appropriate profile design. Attachment-line contamination and instability (Pfenninger 1977; Poll 1985) can originate from leading-edge radius and sweep angle, and can be controlled by keeping the leading-edge radius below a critical value. Streamwise instabilities related to the Tollmien-Schlichting mechanism typically occur in the mid-chord region (Reed et al. 1996), but they can be easily controlled using a favorable

pressure gradient and minimizing the extent of the pressure-recovery region. The last source of boundary-layer instabilities on a swept wing is the crossflow originating from an imbalance between centripetal acceleration and pressure gradient. As a consequence, the favorable pressure gradients used to stabilize streamwise instabilities destabilize the crossflow. For years, the only solution to crossflow control was thought to be surface suction. However, the complications and additional maintenance were always discouraging factors. On the contrary, passive laminar flow control, like the one proposed in this work for a supersonic swept wing, seems to be more feasible and more easily and directly realizable in the airplane industry.

1.2 Excitation of primary crossflow instability

The excitation of the crossflow instability passes trough the receptivity mechanism, which allows the external disturbances to enter the boundary layer and grow. Different sources like freestream turbulence, surface roughness, or their interaction, can play a significant role in the receptivity of 3-D boundary layers.

As far as the role of freestream fluctuations is concerned, experiments by Deyhle and Bippes (1996) showed that for low levels of freestream turbulence, the transition mechanism is dominated by stationary crossflow waves, while at high disturbance levels, traveling waves dominate because of the larger-amplitude, unsteady initial conditions. These traveling waves can overshadow the stationary structure. However, the stationary modes may be the most important in practical cases, due to the low freestream turbulence observed in flight situations.

Surface roughness is the other important crossflow receptivity mechanism. Configurations tested at ASU for the low-speed case, in a low-disturbance freestream environment and stationary-wave-dominated boundary layer, include distributed random roughness and isolated static roughness elements (Radeztsky et al. 1999), and spanwise-periodic, static roughness arrays (Reibert et al. 1996). For random, natural-surface roughness, dramatic transition improvements were obtained by decreasing the rms roughness level. For instance, for a chord Reynolds number $Re_c = 2.4$ million, decreasing the rms roughness from 3.3 μm to 0.2 μm delayed transition from 45% to 65% chord. The isolated roughness element studies showed that stationary crossflow features are generated by particular 3-D roughness elements at 1–3% chord near the first neutral point of the crossflow instability – small 3-D roughness placed further downstream and 2-D roughness both have no effect. The most effective spanwise scale for an isolated roughness element is about one-fourth the most amplified stationary crossflow wavelength.

From the primary instability studies, for which spanwise-periodic roughness arrays were used, a number of crossflow-transition features were established. Reibert et al. (1996) showed that primary stationary waves quickly undergo nonlinear evolution. Nonlinearities seem to be important because they transfer $O(1)$ momentum and produce a large integrated effect in the streamwise direction, even if the stationary disturbances are small. This results in a strongly distorted mean flow and a subsequent saturation of the primary wave and growth of harmonics. Saturation appears before transition and the saturation amplitude seems to be independent of the leading-edge roughness amplitude. When the primary wavenumber disturbance saturates, a rich spectrum of harmonics of the primary are produced, but no subharmonics appear (harmonics and subharmonics in wavenumber space). Excellent agreement between the NPSE (nonlinear parabolized stability equations) computations of Reed et al. (1998) and Haynes and Reed (2000) and the experiments of Reibert et al. (1996) and Saric et al. (1998b) has been found, suggesting that all the features important for the primary instability, including curvature and details of the nonlinear effects, are correctly modeled.

Flow-visualization studies by Dagenhart & Saric (1999), regarding stationary wave dominated transition experiments, proved that the final stage of transition occurs over a very

short streamwise distance and is the result of a secondary instability. This means that transition to turbulence occurs very rapidly at some point downstream of where the vortices saturate. This behavior was initially described experimentally by Kohama et al. (1991) and Kawakami et al. (1999) and analytically/computationally by Malik et al. (1994, 1996, 1999) and Janke and Balakumar (2000). Recent DNS work by Wasserman and Kloker (2002) and experimental work by White and Saric (2002) has put the secondary instability on firm ground.

2 INFRARED THERMOGRAPHY

2.1 The use of IRT for transition detection

Laminar-to-turbulent boundary-layer transition is very sensitive to environmental disturbances. For this reason, when transition-detection is the main goal of an experimental study, particular attention should be paid in order to use a non-intrusive measurement technique. IRT is probably the least intrusive technique because it does not require any kind of modification or interaction with the model or the flow, which could alter the phenomenon under investigation. In some cases, if a better image contrast is needed, the model can be heated or cooled with respect to its natural temperature, making IRT more intrusive. In general, however, IRT does not need any model or flow alterations and is completely non-intrusive.

The basic principle behind the use of IRT for transition-detection is differences in the heat-transfer coefficients between laminar and turbulent flows. The laminar boundary layer allows very low heat exchanges between the model surface and the surrounding freestream flow. Laminar regions are characterized by a very low heat-transfer coefficient and behave as a good insulator. In practice, this means that the surface has the tendency to keep its initial temperature, which, in general, is different from the temperature of the external flow. On the contrary, the turbulent boundary layer features high mixing and therefore high heat exchange. As a direct consequence, a surface characterized by a turbulent boundary layer will reach the temperature of the surrounding, incoming flow faster than a laminar boundary layer.

In a blow-down supersonic wind tunnel two possible scenarios can be foreseen: the initial model temperature is lower than the external flow, or the initial model temperature is higher. The case in which the model and the external flow have the same temperature is quite an uncommon event and is not interesting since no difference between laminar and turbulent regions can be appreciated due to the lack of heat exchange between the surface and the freestream flow. If the model is colder than the incoming flow, laminar-flow regions will appear as cold spots on the infrared image. The reason, as previously explained, is that the laminar boundary layer is a very good insulator and keeps the model at its original temperature. On the other hand, turbulent-flow regions will appear warmer since the high heat exchange will allow the model to easily reach the external higher temperature. The case of a model warmer than the incoming flow is reversed: laminar regions are warmer than turbulent ones.

The other advantage of using IRT for transition detection, besides its non-intrusive nature, is that a global flow-field image is obtained without the necessity of multiple local measurements. However, if local information is needed, data can be retrieved from the whole image using the post-processing software that comes with the most common IR cameras used for scientific purposes.

2.2 Problems encountered using IRT

Infrared thermography tests were conducted with a FLIR 3000 camera that was mounted inside the tunnel in a cavity above the model. The camera was therefore directly exposed to the

model and the flow, without an intermediate window. This was done because one of the most common problems when using IRT in a wind tunnel is the window through which the camera is detecting the radiation coming from the model. The spectral range of the camera is 8-9μm and the detector is 320x240 pixels, cooled to 70 K.

The main difficulty we had to deal with were reflections coming from the cavity where the IR camera was set. In fact, the IR camera produces a lot of heat when operating and thus the flow in the cavity is much warmer than the flow in the test section. The radiation reflected by the model is clearly not related to its temperature and is therefore misleading when surface-temperature differences are searched for. Reflectivity is a characteristic of the surface, and in our case it is required to be very smooth and polished in order to avoid surface roughness playing an unexpected role. A very well polished, metal model is probably the best candidate for a high reflectivity coefficient. The result is an IRT image in which a hot region is detected. This is obviously an artificial result: that high temperature region is not physically present on the model, but it corresponds to the reflected image from the warm cavity. If other materials are used, like phenolic (or bakelite), reflections from the surroundings are strongly reduced and differences in the temperature of the surface are more visible thanks to low heat conductivity. A trick that we used in order to avoid the cavity reflection on the model is to set the camera so that its line-of-sight is not perpendicular to the surface but has an angle with respect to the normal from the surface.

Another problem related to IRT is the initial temperature distribution (before starting the tunnel). It has been estimated that the temperature difference between a laminar and a turbulent boundary layer is on the order of 2-3° C. This means that to be able to detect this temperature difference, the initial temperature distribution must be, ideally, within less than O(2-3° C). One straightforward possibility is to keep the test section closed, with the model inside, for some time before running the tunnel. However, since the tunnel is a blow-down-to-atmosphere facility, the test section is directly connected to the outside and its temperature is very sensitive to the atmospheric temperature. As a result, the part of the model closer to the wind tunnel outlet is always at a different temperature with respect to the part further away from the outlet.

Another problem is usually the emissivity of the material, which should be measured as it depends on several factors. For our tests, since we are more interested in the temperature difference between different regions on the surface, rather than their exact absolute temperature, the emissivity is assumed to be the tabulated value for that particular material.

3 EXPERIMENTAL FACILITY

3.1 The Supersonic Wind Tunnel

All the experiments are carried out at the ASU 0.2-meter Supersonic Wind Tunnel. This is a blow-down-to-atmosphere facility with nozzle blocks for Mach 2.4, 3.0. 3.5 and a test section size of 0.20 m x 0.18 m. The reservoir pressure is $3.45\cdot10^6$ Pa (500 psia) and the tunnel can be started with a settling chamber pressure of $2.74\cdot10^5$ Pa (25 psig) corresponding to a unit Reynolds number Re'= $28.5\cdot10^6$/m (Re'= $8.7\cdot10^6$/ft). It has been operated up to a settling chamber pressure of $5.15\cdot10^5$ Pa (60 psig).

Particle filters, dryers, and screens are used to improve the flow quality. At the entrance of the 0.61-m-diameter settling chamber, there are four 30-mesh turbulence-reduction screens each with an open area ratio of 65%. After the settling chamber, a circular-to-rectangular transition contracts the flow into the subsonic portion of the 2-D convergent-divergent nozzle. Two nozzle

blocks form the upper and lower contours of the supersonic nozzle and provide a test section of approximately 0.18x0.20 m. Both the upper and lower blocks have rectangular access ports in the test section for the installation of instrumentation.

The tunnel is controlled using LabView software running on a standard Intel P-III 800 MHz MS Windows based PC. Data acquisition is accomplished using two PCI DAQ boards. One of the boards has 16 channels (single-ended) and can sample at a maximum frequency of 333 KHz. It has two analog outputs, which are used to control the valves in response to changes in the stagnation pressure reading. The second board provides four channels (differential) and is used for hotwire/high-speed data acquisition because it can sample at a maximum frequency of 5 MHz.

The wind tunnel is equipped also with a Schlieren imaging system (which can function in a shadowgraph mode too) to visualize shock and expansion waves in the test section.

Because of the fact that crossflow instability is not sensitive to sound, the ASU tunnel is suitable for this kind of investigations.

4 WIND TUNNEL MODELS

Different wind-tunnel models (geometries and materials) were tested. A short description, for three of them, is here provided.

Fig. 1 - 73° swept-wing aluminum model

Fig. 2 - 50° swept-wing phenolic model

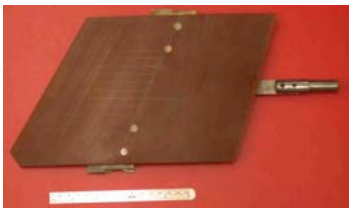

Fig. 3 - 30° swept-wing phenolic model

4.1 The 73° swept-wing model

In order to minimize loads in the experiments, a symmetric shape is used. Referring to the picture reported in Fig. 1, this wing is features a 73º leading-edge sweep angle, 0.3048 m (12”) mid-span, streamwise chord, and t/c= 4%. The trailing edge sweep is 71.2º, the root chord is 339 mm (13.35″), and the tip chord is 271 mm (10.67″). The attachment line Reynolds number is *O*(40), well below 100 to avoid attachment-line contamination.

The model can be mounted vertically, or horizontally, depending on the type of tests needed. The vertical set-up was used in order to prove that there are no shock waves generated by the leading edge, since a 73° sweep angle at M=2.4 provides a subsonic leading edge. In the horizontal position, two configurations are possible: the model can be close to the floor or in the middle of the tunnel. The reason for this difference is that the hotwire traverse and infrared camera are both mounted on the ceiling of the tunnel (never simultaneously). However, when dealing with hotwire measurements, the length of traverse sting exposed to the supersonic flow should be kept as short as possible in order to reduce the aerodynamic load on the structure. On the other hand, when dealing with infrared thermography, a larger field of view is preferable, and therefore the model is mounted as far as possible from the camera.

The model shown in Fig. 1 is made of aluminum and powder-coated with a 76 μm thick coating. This was done in order to provide a better insulation between the model and flow. In fact, aluminum has a very high thermal conductivity and therefore the temperature difference due to laminar-to-turbulent transition could easily disappear.

Another way to reduce the "wash-out" effect due to the high thermal conductivity of aluminum was to build a model with the same geometric characteristics, but made of phenolic. This material is commonly known as Bakelite and since it is very similar to a plastic its thermal conductivity is very low.

4.2 The 50° swept-wing model

The 50° wept-wing model is made of black phenolic (see Fig. 2). It features a leading edge sweep of 50° and trailing edge sweep of 48°. The root chord is 147 mm (5.8″), and the tip chord is 135 mm (5.3″). It is a very thin airfoil, with t/c= 3%. This wing is characterized by a supersonic leading edge because the leading-edge sweep-angle is smaller than the Mach angle. A shock, therefore, originates from the leading edge. The model is mounted at about 44 mm from the floor (1.75").

4.3 The 30° swept-wing model

The 30° wept-wing model is made of brown phenolic (see Fig. 3). The leading edge sweep is 30° and the trailing edge sweep 18°; the root chord 254 mm (10″), and the tip chord is 211 mm (8.3″). This is the thickest wing tested in our Supersonic Wind Tunnel, with t/c= 6%. As for the 50° model, the leading edge is supersonic. The wing is mounted along the wind-tunnel centerline through a sting from the back and two lateral supports, as shown in Fig. 3.

5 RESULTS

Different initial model temperatures were tested: cold, hot and ambient. In the first case, the model is cooled using liquid nitrogen. However, since this is a manual operation with the model already in place, we found very difficult to achieve an accurate uniformity in the initial temperature distribution. On the other hand, the idea behind a hot model is to increase the surface temperature and therefore the radiation coming from the model itself, reducing the reflections. Ambient temperature tests, in general, look very close to hot model tests because the ambient temperature is usually about 21° C or higher, while the flow temperature during the run is always below 15° C.

5.1 The 73° swept-wing model

Fig. 4 shows the IRT image of the 73° swept-wing cold model, M=2.4, $Re=9.7\cdot10^6$, flow left to right. In this test, control dots, 0.5 mm diameter, 6-μm high elements at 1.7 mm spacing are placed in the vicinity of the leading edge as reported on the figure. Their purpose is to control the crossflow instability. A large roughness element is also located close to the leading edge in order to trip the boundary layer. The wake behind the latter does not spread as a turbulence wedge meaning that the flow is probably turbulent even close to the leading edge. A reflected wave also

seems to appear. It could be the Mach wave originating from the leading edge at the root and then reflecting on the opposite wind-tunnel wall. The cold spot in the center of the image is the reflection of the camera detector (which is at very low temperature), while the hot region is the

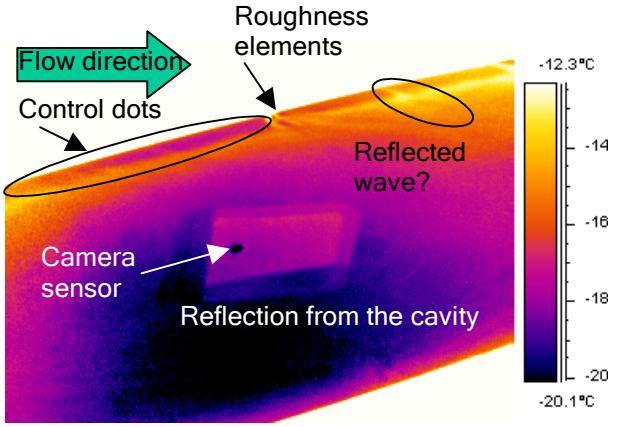

Fig. 4 - 73° swept-wing aluminum model. M=2.4; Re=9.3·10^6; cold. Flow left to right

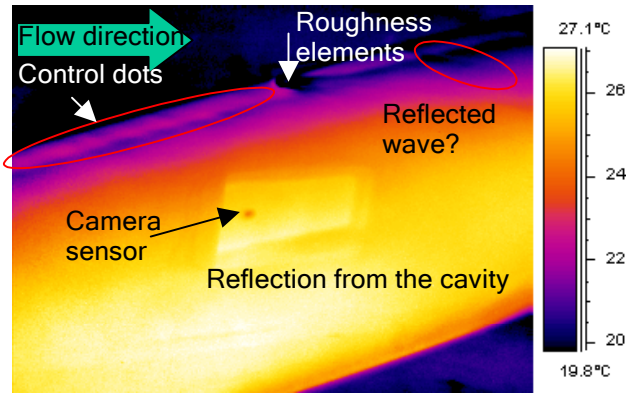

Fig. 5 - 73° swept-wing aluminum model. M=2.4; Re=9.3·10^6; warm. Flow left to right

reflection of the cavity where the camera is located. The cold region behind 50% chord is due to a non-uniform temperature distribution when the model is cooled with liquid nitrogen.

Fig. 5 is referred to the same conditions as Fig. 4, but the model is hot instead of cold. Some improvements are made with respect to Fig. 4. First the reflection from the cavity seems to be weaker, thanks to the fact that the model is at a higher temperature. Second, at the leading edge structures similar to streaks can be clearly identified.

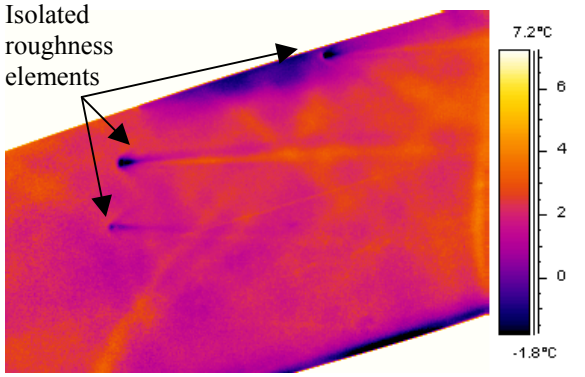

Fig. 6 - 73° swept-wing, phenolic model. M=2.4; Re=9.3·10^6; α=–5°; ambient. Flow left to right

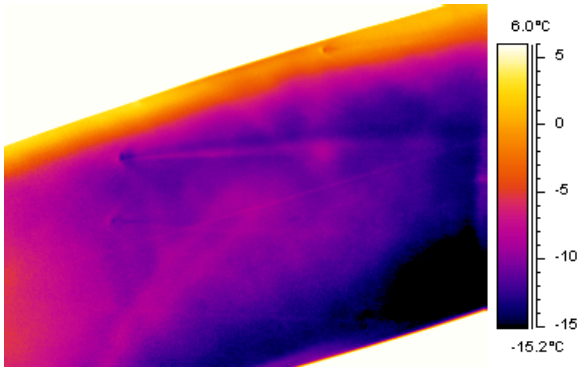

Fig. 7 - 73° swept-wing, phenolic model. M=2.4; Re=9.3·10^6; α=–5°; cold. Flow left to right

In Fig. 6 a test in ambient conditions on the phenolic model is shown for an angle of attack α= -5°. Three huge isolated roughness elements are set on the wing. In all cases the flow behind them shows a characteristic narrow wake, typical of turbulent flows. In other words, the roughness elements are in turbulent regions, even the disturbance on the leading edge, meaning that the whole flow field on the wing is turbulent. As clearly visible on the temperature scale on the right-hand-side, Fig. 7 differs from Fig. 6 only because the model was cold, instead of at ambient temperature. Besides the turbulent wakes behind the distributed roughness elements, an important feature is that the leading edge appears much warmer than the rest of the wing. This occurs because of the thinner thickness of the model in proximity of the leading edge, which allows a faster temperature recovery (the external flow is warmer than the model). The fact that

the leading edge is warmer is therefore not related to transition phenomena, because the complete flow field looks turbulent.

5.2 The 50° swept-wing model

Results from the 50° swept-wing are shown in Fig. 8 (ambient) and Fig. 9 (cold). The angle of attack is α= -1°, M=2.4, Re'=29.4·10^6/m, Re=4.15·10^6, flow left to right. In Fig. 8 a transition front is clearly visible at about 17% chord. It looks very uniform, except for the turbulent wedge due to the roughness element on the leading edge and a couple of very small wedges coming

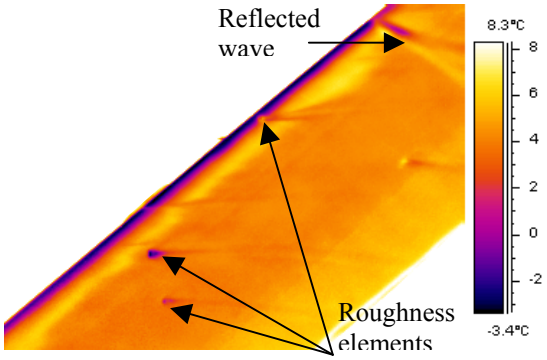

Fig. 8 - 50° swept-wing, phenolic model. M=2.4; Re=4.15·10^6; α=–1°; ambient. Flow left to right

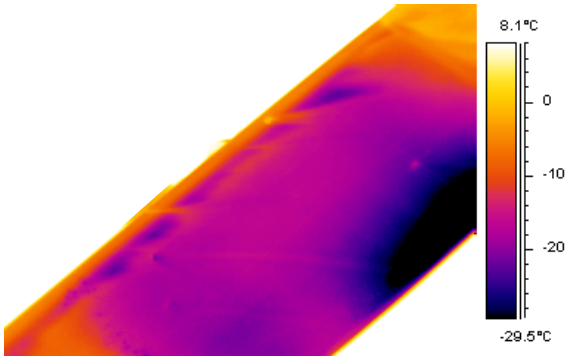

Fig. 9 - 50° swept-wing, phenolic model. M=2.4; Re=4.15·10^6; α=–1°; cold. Flow left to right

from two dings on the leading edge. A reflected wave is also visible in the upper-right portion of the image. The laminar-to-turbulent transition front is characterized by a clear transition from a warm region at about 7.5° C (laminar) to a colder region at about 4.5° C (turbulent). As explained in section 2.1, since the external flow is at a lower temperature than the model, and the laminar boundary layer is a good insulator, the laminar region looks warmer than the turbulent one. The leading edge is much colder than the rest of the model. This occurs not because of a turbulent flow, but simply because of its very low thermal inertia, which lets it reach the external, lower temperature much faster.

Fig. 9 regards the same conditions as in Fig. 8, but the model was cooled with liquid nitrogen before running the test so that its temperature is lower than the external flow. The colors are reversed with respect to ambient conditions. The laminar region is now cold because the laminar boundary layer, as an insulator, keeps the original low temperature of the model. Transition to turbulence, therefore, appears as cold-to-warm transition. The portion of the wing beyond 30% chord looks cold because the model is thicker there, the thermal inertia is higher and it takes longer to reach the external flow temperature. In contrast with Fig. 8, the leading edge now is warm with respect to the rest of the model and it goes without saying that the reason is its low thermal inertia.

5.2 The 30° swept-wing model

Fig. 10 and Fig. 11 shown transition detected on the 30° swept wing, made of phenolic, for two different angles of attack, cold models. Referring to Fig. 10, at α=0°, the transition front can be undoubtedly identified. Since the model was cooled to -40° C, laminar-to-turbulent transition

appears as cold-to-warm transition. The leading edge is warmer than the laminar region only because of its thin thickness. The turbulent wedges are due to small disturbances present on the leading edge. No isolated roughness elements were set on purpose on the wing. Fig. 11 shows that when the model is pitched at $\alpha = -0.6°$, the transition front moves downstream, as expected, so that the laminar region extends up to 25% chord.

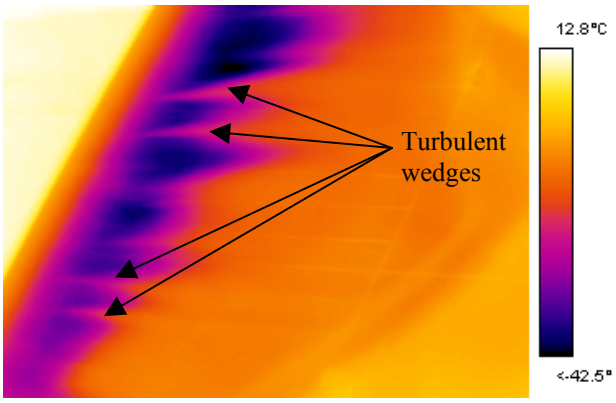

Fig. 10 - 30° swept-wing phenolic model. M=2.4; Re=6.8·10^6; α=0°; cold. Flow left to right

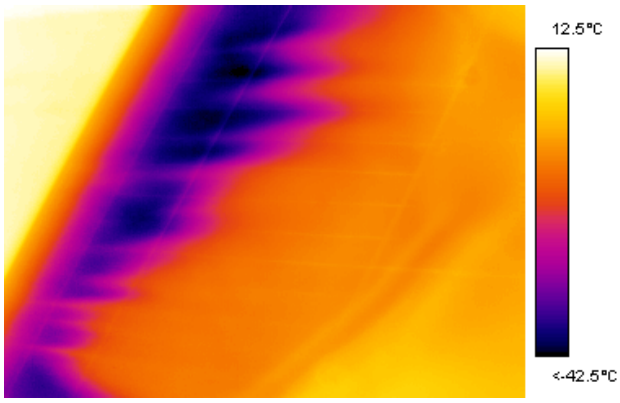

Fig. 11 - 50° swept-wing phenolic model. M=2.4; Re=6.8·10^6; α=–0.6°; cold. Flow left to right

These two images show that, when dealing with laminar-to-turbulent boundary layer transition, IRT can be used as quantitative measurement technique and as a qualitative visualization technique. The main advantage is that, if used at ambient temperature, it does not require any modification of the model surface, as other visualization technique do (naphthalene, heavy-duty-gear oil, tufts).

6 CONCLUSIONS

The original motivation for this study was crossflow-dominated transition on a supersonic swept wing. Infrared thermography has been used on models of different materials and geometries, as a transition-detection tool. When transition occurs, it can easily and clearly be identified on infrared images since the heat transfer between laminar and turbulent boundary layers is different. In particular, when the model is cooled with liquid nitrogen, so that its temperature before the run is lower than the external incoming flow, laminar regions are cold and turbulent regions are warm. This is due to the low heat exchange allowed by the laminar boundary layer, which acts as an insulator. When interpreting the colors and the temperatures on the IR image, particular attention should be paid to the leading edge because its thermal capacity is very low and its temperature cannot be taken as a measure of laminar/turbulent flow.

In summary, results presented in this paper prove that infrared thermography is a very well suited tool for transition detection. It can be used as a measurement or visualization technique, is totally non-intrusive and provides a global picture of the entire flow-field.

ACKNOLEDGMENTS

The work was supported by the DARPA QSP program under Grant MDA972-01-2-0001. The help and practical suggestions of Mr. Dan Clevenger during the experiments have been very appreciated.

REFERENCES

1. Arnal, D. 1997 Laminar-turbulent transition: Research and applications in France. *AIAA Paper 97-1905*.
2. Bippes, H. 1997 Environmental conditions and transition prediction in 3-D Boundary layers. *AIAA Paper 97-1906*.
3. Bippes, H. 1999 Basic experiments on transition in three-dimensional boundary layers dominated by crossflow instability. *Prog. Aero. Sci. 35*, 363-412.
4. Crouch, J.D. 1997 Transition prediction and control for airplane applications. *AIAA Paper 97-1907*.
5. Dagenhart, J.R., Saric, W.S. 1999 Crossflow stability and transition experiments in swept-wing flow. *NASA/TP-1999-209344*.
6. Deyhle, H. & Bippes, H. 1996 Disturbance growth in an unstable three-dimensional boundary layer and its dependence on initial conditions. *J. Fluid Mech. 316*, 73-113.
7. Gladden, R.D. 2001 *Crossflow transition in elevated freestream turbulence*. M.S. Thesis, Arizona State University, December 2001.
8. Haynes, T.S., Reed, H.L. 2000 Simulation of swept-wing vortices using nonlinear parabolized stability equations. *J. Fluid Mech. 405,* 325-49.
9. Herbert, Th. 1997a On the stability of 3-D boundary layers. *AIAA Paper 97-1961*.
10. Herbert, Th. 1997b Transition prediction and control for airplane applications. *AIAA Paper 97-1908*.
11. Janke, E., Balakumar, P. 2000 On the secondary instability of three-dimensional boundary layers. *Theoret. Comput. Fluid Dynamics 14*, 167-94.
12. Kachanov, Y.S. 1996 Experimental studies of three-dimensional instability of boundary layer. *AIAA Paper 96-1976*.
13. Kawakami, M., Kohama, Y. Okutsu, M. 1999 Stability characteristics of stationary crossflow vortices in three-dimensional boundary layer. *AIAA Paper 99-0811.*
14. Kohama, Y., Saric, W.S., Hoos, J.A. 1991 A high-frequency, secondary instability of crossflow vortices that leads to transition. *Proc. of the Royal Aero. Soc. Conf. on Boundary-Layer Trans. and Control* .
15. Malik, M.R., Li, F., Chang, C.L. 1994 Crossflow disturbances in three-dimensional boundary layers: Nonlinear development, wave interaction and secondary instability. *J. Fluid Mech. 268*, 1-36.
16. Malik, M.R., Li, F., Chang, C.L. 1996 Nonlinear crossflow disturbances and secondary instabilities in swept-wing boundary layers. In IUTAM Symposium on Nonlinear Instability and Transition in Three-Dimensional Boundary Layers (ed. P. W. Duck & P. Hall), pp. 257-66. Kluwer.
17. Malik, M.R., Li, F., Choudhari, M.M. Chang, C.L. 1999 Secondary instability of crossflow vortices and swept-wing boundary layer transition. *J. Fluid Mech. 399*, 85-115.
18. Pfenninger, W. 1997 Laminar flow control – Laminarization. *AGARD Report No. 654.*
19. Poll, D.I.A. 1985 Some observations of the transition process on the windward face of a long yawed cylinder. *J. Fluid Mech. 150*, 329-56.
20. Radeztsky, R.H., Reibert, M.S., Saric, W.S. 1999 Effect of isolated micron-sized roughness on transition in swept-wing flows. *AIAA J.*, *37* (11), 1370-77.
21. Reed, H.L., Saric, W.S. 1989 Stability of three-dimensional boundary layers. *Annu. Rev. Fluid Mech. 21*, 235-84.
22. Reed, H.L., Saric, W.S., Arnal, D. 1996 Linear stability theory applied to boundary layers. *Annu. Rev. Fluid Mech. 28,* 389-428.

23. Reed, H.L., Saric, W.S., Haynes, T.S. 1998 CFD validation issues in transition modeling. *AIAA J. 36* (5) 742-51.
24. Reibert, M.S., Saric, W.S., Carrillo, Jr., R.B., Chapman, K.L. 1996 Experiments in nonlinear saturation of stationary crossflow vortices in a swept-wing boundary layer. *AIAA Paper 96-0184*.
25. Reibert, M.S., Saric, W.S. 1997 Review of swept-wing transition. *AIAA Paper 97-1816*.
26. Reshotko, E. 1997 Progress, accomplishments and issues in transition research. *AIAA Paper 97-1815*.
27. Saric, W.S. 1994 Görtler vortices. *Annu. Rev. Fluid Mech. 26*, 379-409.
28. Saric, W.S., Carrillo, Jr., R.B., Reibert, M.S. 1998a Nonlinear stability and transition in 3-D boundary layers. *Meccanica 33*, 469-87.
29. Saric, W.S., Carrillo, R.B., Reibert, M.S. 1998b Leading-edge roughness as a transition control mechanism. *AIAA Paper No. 98-0781*.
30. Wasserman, P., Kloker, M. 2002 Mechanisms and control of crossflow-vortex induced transition in a three-dimensional boundary layer. *J. Fluid Mech*. In press.
31. White, E.B., Saric, W.S. 2000 Application of variable leading-edge roughness for transition control on swept wings. *AIAA Paper No. 2000-0283*.
32. White, E.B., Saric, W.S. 2002 Secondary instability of crossflow vortices. *J. Fluid Mech.* In press.